PHYSICAL REVIEW D **86,** 014033 (2012)

Single spin asymmetry through QCD instantons

Yachao Qian and Ismail Zahed

Department of Physics and Astronomy, Stony Brook University, Stony Brook, New York 11794-3800

(Received 24 April 2012; published 27 July 2012)

We revisit the effects of QCD instantons in semi-inclusive deep inelastic scattering. We show that large single spin asymmetry (SSA) effects can be induced in longitudinally and transversely polarized proton targets. The results are in agreement with most of the reported data for pion and kaon production. The same effects are found to be important in polarized proton on proton scattering for both charged and chargeless pion productions. The results agree with the reported data in a wide range of $\sqrt{s} = 19.4$–200 GeV. We predict the SSA for $\pi^{\pm}$ production in $p_{\uparrow}p$ in the collider range of $\sqrt{s} = 62.4$–500 GeV. The backward $\pi^{\pm}$ and π^0 productions for the SSA in $p_{\uparrow}p$ collisions are predicted to coincide at large $\sqrt{s}$.

DOI: 10.1103/PhysRevD.86.014033 PACS numbers: 13.88.+e, 11.30.Rd

I. INTRODUCTION

QCD instantons play a central role in the spontaneous breaking of chiral symmetry in the QCD vacuum, and may contribute significantly to the spectroscopic properties of the low lying hadrons [1,2]. They may also contribute substantially to semihard scattering processes by accounting for the soft pomeron physics [3–7] and possibly gluon saturation at HERA [8,9]. Recent lattice gauge simulations may support these claims [10].

The QCD instanton intrinsic spin-color polarization makes them ideal for generating nonperturbative and large spin asymmetries in deep inelastic scattering using polarized proton targets [11–14]. Dedicated single spin asymmetry (SSA) experiments in both semi-inclusive deep inelastic scattering (SIDIS) using $lp_{\uparrow} \to l'\pi X$ by the CLAS and HERMES collaborations [15–18], as well as polarized proton on proton scattering using $p_{\uparrow}p \to \pi X$ by the STAR and PHENIX collaborations [19–22] have unraveled large spin dependent effects.

The large spin asymmetries observed experimentally are triggered by T-odd contributions in the scattering amplitude. Since perturbative QCD does not accommodate these effects, it was initially suggested that these T-odd contributions are either induced in the initial state (Sivers effect) [23] or in the fragmentation function (Collins effect) [24,25] thereby preserving the integrity of QCD perturbation theory and factorization. QCD instantons offer a natural mechanism for generating T-odd amplitudes that is fully rooted in QCD and beyond perturbation theory [12–14]. This approach will be pursued below.

The organization of the paper is as follows: In Sec. II we revisit and correct the effects of the single instanton on the T-odd contribution for the cross section in SIDIS as suggested in [14]. We derive the azimuthal spin asymmetry for longitudinally polarized targets and the Sivers amplitude for transversely polarized targets. By assuming the instanton parameters to be fixed by their vacuum values, we find good agreement with pion and kaon production [15–18]. In Sec. III we extend our analysis to $p_{\uparrow}p$ collisions and compare to the pion production results reported by STAR and PHENIX [19–22]. Our results agree with the experimentally measured SSA for π^0 production in a wide range of $\sqrt{s}$. We predict the SSA for both forward and backward charged pion in $p_{\uparrow}p$ collisions for a broad range of collider energies. Remarkably, π^0 and $\pi^{\pm}$ productions are found to coincide backward at large $\sqrt{s}$. Our conclusions are in Sec. IV. Some pertinent calculational details can be found in the Appendices.

II. SEMI-INCLUSIVE DEEP INEALSTIC SCATTERING

To set up the notations for the semi-inclusive processes in deep inelastic scattering, we consider a proton at rest in the LAB frame with either longitudinal or transverse polarization as depicted in Fig. 1. The incoming and outgoing leptons are unpolarized. The polarization of the target proton in relation to the DIS kinematics is shown in Fig. 2. Throughout, the spin dependent asymmetries will be evaluated at the partonic level. Their conversion to the hadronic level will follow the qualitative arguments presented in [12–14].

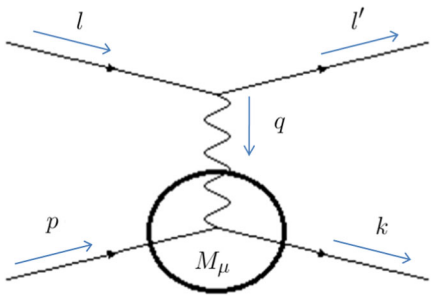

FIG. 1 (color online). l and l' denote the momentum for the incoming and outgoing lepton. p and k are the momenta of the incoming and outgoing quark. The lepton and the quark exchange one photon in the single instanton background.

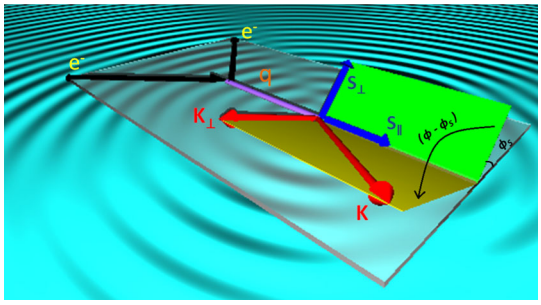

FIG. 2 (color online). The lepton and photon are in the same plane. The angle between the transversely polarized spin $s_\perp$ and this plane is ϕ_s. The angle between the transversely spatial momentum $K_\perp$ of the outgoing pion and the plane is ϕ. The convention for azimuthal angle is consistent with experiments.

A. One instanton contribution

Generically, the spin averaged leptonic tensor reads

$$L^{\mu\nu} = \frac{1}{2}\,\mathrm{tr}[l'\gamma_\mu l\gamma_\nu], \tag{1}$$

while the color averaged hadronic tensor in the one instanton background reads

$$W_{\mu\nu} = \sum_{\text{color}} \frac{1}{2}\,\mathrm{tr}[kM_\mu p(1+\gamma_5 s)M_\nu] \tag{2}$$

with the constituent vertex

$$M_\mu = \gamma_\mu + M_\mu^{(1)} \tag{3}$$

that includes both the perturbative γ_μ and the nonperturbative insertion $M_\mu^{(1)}$.

In general, $W_{\mu\nu}^{(1)}$ admits all possible tensor structures compatible with gauge and parity invariance, for a fixed proton spin s^μ. For the Sivers effect to be considered below, there are only *two* tensor combinations of interest:

$$p_\mu \epsilon_{\nu abc} s^a k^b p^c \quad \text{and} \quad q_\mu \epsilon_{\nu abc} s^a k^b p^c.$$

The last tensor combination contracts to zero leptonically. Therefore $W_{\mu\nu}^{(1)}$ can only support the first tensor combination $p_\mu \epsilon_{\nu abc} s^a k^b p^c$. This tensor structure is due to the chirality flip vertex $M_\mu^{(1)}$ induced by a single instanton. It is at the origin of the SSA in the hard scattering amplitudes to be derived below. In Appendix A we detail its derivation following the original arguments in [14,26]

$$M_\mu^{(1)} = i\frac{4\pi^2\rho^2}{\lambda Q^2}[\gamma_\mu k + p\gamma_\mu](1 - f(\rho Q)) \tag{4}$$

with $f(a) = aK_1(a)$ and after color averaging. Here ρ is the instanton size and λ the renormalized virtuality of the instanton quark zero mode. Both of these parameters will be discussed below using the QCD instanton vacuum.

The leading nonperturbative instanton contribution to (8) is a cross contribution in the hadronic tensor (2) after inserting the one-instanton vertex (4)

$$\begin{aligned} W_{\mu\nu}^{(1)} &= \frac{1}{2}\,\mathrm{tr}[kM_\mu^{(1)} p\gamma_5 s\gamma_\nu] + (\mu \leftrightarrow \nu) \\ &= \frac{16\pi^2\rho^2}{\lambda Q^2}(1 - f(\rho Q))(p+k)_{\{\mu}\epsilon_{\nu\}abc} s^a k^b p^c, \end{aligned} \tag{5}$$

where the short notation $(\cdots)_{\{\mu}\epsilon_{\nu\}abc} \equiv (\cdots)_\mu \epsilon_{\nu abc} + (\cdots)_\nu \epsilon_{\mu abc}$ is used. If we set $p = xP$ and $k = K/z$ and note that $p + k = 2p + q$, then (5) simplifies

$$W_{\mu\nu}^{(1)} = \frac{2^5\pi^2\rho^2}{\lambda Q^2}\frac{x^2}{z}(1 - f(\rho Q))\left(P + \frac{q}{2x}\right)_{\{\mu}\epsilon_{\nu\}abc} s^a K^b P^c. \tag{6}$$

Combining (1) and (6) yields

$$\begin{aligned} W_{\mu\nu}^{(1)} L^{\mu\nu} = \frac{2^7\pi^2\rho^2}{\lambda Q^2}\frac{x^2}{z}(1 - f(\rho Q)) \\ \times M[E\epsilon_{\nu abc} l'^\nu s^a K^b P^c \\ + E'\epsilon_{\nu abc} l^\nu s^a K^b P^c], \end{aligned} \tag{7}$$

where E (E') is the energy of the incoming (outgoing) (anti)electron.

The normalized lepton-hadron cross section of Fig. 1 follows in the form

$$\frac{d\sigma}{dxdydzd\phi} = y\frac{\alpha^2}{Q^6} L^{\mu\nu} W_{\mu\nu} \sum_i e_i^2 f_i(x, Q^2) D_i(z) \tag{8}$$

with $y = P\cdot q/P\cdot l$, where e_i is the i-parton electric charge, f_i its momentum fraction distribution, and D_i its fragmentation function. The perturbative contribution follows by setting $M_\mu \approx \gamma_\mu$, leading to

$$\frac{d^{(0)}\sigma}{dxdydzd\phi} = N_c\frac{\alpha^2}{Q^2}\frac{1 + (1-y)^2}{y}\sum_i e_i^2 f_i(x, Q^2) D_i(z), \tag{9}$$

where $N_c = 3$ is the number of colors. The sum is over the electrically charged quarks.

The leading instanton contribution to the total cross section (8) follows by inserting (7) into (2). For the target proton polarization set up of Fig. 2, the longitudinal ($\|$) and transverse ($\perp$) cross sections contribute to the total cross section as

$$\begin{aligned} \frac{d^{(1)}\sigma}{dxdydzd\phi} = \alpha^2 \sum_q \frac{32\pi^2\rho^2 e_q^2 D_q(z)}{z\lambda Q^4} K_\perp (1 - f(\rho Q)) \\ \times \left[\frac{\Delta_\| q_q}{2}\left(\frac{2}{y} - 1\right)\sqrt{1 - \frac{y^2}{4} - \frac{x^2y^2M^2}{Q^2}}\sin\phi \right. \\ \left. + \frac{\Delta_\perp q_q}{2}\frac{y}{2}\sqrt{1 + \frac{4M^2x^2}{Q^2}}\sin(\phi - \phi_s)\right], \end{aligned} \tag{10}$$

where $\Delta_\| q_q(x, Q^2)/2 = s_\| f_q(x, Q^2)$ is the spin polarized distribution function for the quark in the longitudinally polarized proton, and $\Delta_\perp q_q(x, Q^2)/2 = s_\perp f_q(x)$ is the spin polarized distribution function for the quark in the transversely polarized proton. Note that $(s_\perp)_{\max} = (s_\|)_{\max} = 1/2$, and

$\Delta q_q(x, Q^2)$ is the distribution function normalized to 1. For further comparison with experiment, we will assume (see HERMES [27]) that $\Delta_\parallel q_q(x, Q^2) = \Delta_\perp q_q(x, Q^2)$ and define the spin structure function

$$g_1(x, Q^2) = \frac{1}{2}\sum_q e_q^2(\Delta q_q(x, Q^2) + \Delta\bar{q}_q(x, Q^2)). \quad (11)$$

Since we are only interested in the SSA in hard scattering processes, we set $D_q(z) = 1$. A comparison of (9) with (10), yields for the longitudinal spin asymmetry (part proportional to $\sin\phi$)

$$A_{UL}^{\sin\phi} = \frac{16\pi^2\rho^2}{N_c Q\lambda}(1 - f(\rho Q))\frac{K_\perp}{zQ}\frac{(2-y)\sqrt{1-\frac{y^2}{4}-\frac{x^2y^2M^2}{Q^2}}}{1+(1-y)^2}\frac{g_1}{F_1} \quad (12)$$

with $F_1(x) = \frac{1}{2}\sum_q e_q^2 f_q(x)$. The same comparison yields for the transverse spin asymmetry [part proportional to $\sin(\phi - \phi_s)$]

$$A_{UT}^{\sin(\phi-\phi_s)} = \frac{8\pi^2\rho^2}{N_c Q\lambda}(1 - f(\rho Q))\frac{K_\perp}{zQ}\frac{y^2\sqrt{1+\frac{4M^2x^2}{Q^2}}}{1+(1-y)^2}\frac{g_1}{F_1}. \quad (13)$$

This is usually referred to as the Sivers contribution.

The longitudinal to transverse ratio simplifies

$$\frac{A_{UL}^{\sin\phi}}{A_{UT}^{\sin(\phi-\phi_s)}} = \frac{2(2-y)\sqrt{1-\frac{y^2}{4}-\frac{x^2y^2M^2}{Q^2}}}{y^2\sqrt{1+\frac{4M^2x^2}{Q^2}}} \quad (14)$$

as the details of the instanton form factor and the partonic distributions drop out. In the hard scattering limit with large Q^2, i.e. $\frac{M^2}{Q^2} \ll 1$, (14) is universal

$$\frac{A_{UL}^{\sin\phi}}{A_{UT}^{\sin(\phi-\phi_s)}} = \frac{2(2-y)\sqrt{1-\frac{y^2}{4}}}{y^2}. \quad (15)$$

B. Results versus data

To compare with SIDIS experiments we need to set up the instanton parameters. The instanton size will be set to its mean value in the QCD vacuum, $\rho \approx 1/3$ fm or $1.7/\text{GeV}$ [1,2]. The mean instanton quark zero mode virtuality is tied to the light quark condensate χ_{uu} through $\bar{\lambda} = 1/\chi_{uu}$. For two flavors $\chi_{uu} \approx (200\ \text{MeV})^3$, so that $\bar{\lambda} \approx 1/(0.2\ \text{GeV})^3$. Thus $16\pi^2\rho^2/N_c\lambda \approx 1.22$ GeV in (12) and (13).

We recall that in the recent CLAS experiment [18] the kinematical ranges are: $Q^2 \approx (0.9\text{–}5.4)\ \text{GeV}^2$, $x \approx (0.12\text{–}0.48)$, $z \approx (0.4\text{–}0.7)$, and $K_\perp \approx (0\text{–}1.12)$ GeV. For comparison, we use the mean values $\langle z\rangle \approx 0.55$ and $\langle K_\perp\rangle \approx 0.56$ GeV. For the spin structure function we use $g_1^p/F_1^p \approx 0.354$ for $(x, Q^2) \approx (0.274, 3.35\ \text{GeV}^2)$ from the tabulated values in [27]. This choice of (x, Q^2) agrees with the averaged values of x and Q^2 as covered by the CLAS experiment [18]. The final result is averaged over the full measurement range of $y \approx (0\text{–}0.85)$. Figure 3 shows our result for the longitudinally polarized spin asymmetry versus azimuth. The data are from the CLAS experiment [18]. There is overall agreement in magnitude and oscillation.

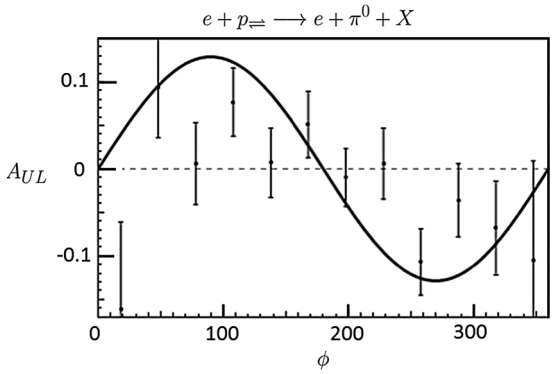

FIG. 3. Longitudinally polarized spin asymmetry versus azimuth ϕ. The data are from [18].

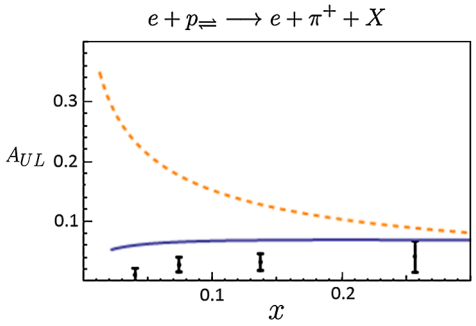

FIG. 4 (color online). Longitudinally polarized spin asymmetry [15]. Our result (12) (solid line) and the result in [14] (dashed line).

The kinematical ranges in the longitudinally polarized HERMES experiment [15] are $\langle K_\perp\rangle = 0.44$ GeV, $\langle z\rangle = 0.48$, and $0.2 < y < 0.85$. As $\langle Q^2\rangle$ is set for each data point, we parametrize by $\sqrt{\langle Q^2\rangle} = 4.3747\langle x\rangle^{0.4099}$ ($R^2 = 0.998$). This kinematical set up is similar to the one adopted in [14] and will facilitate the comparison. The spin structure function in [15] is $g_1^p/F_1^p = 0.9811\langle x\rangle^{0.7366}$ ($R^2 = 0.98$). In Fig. 4 we show our results (solid line) for the

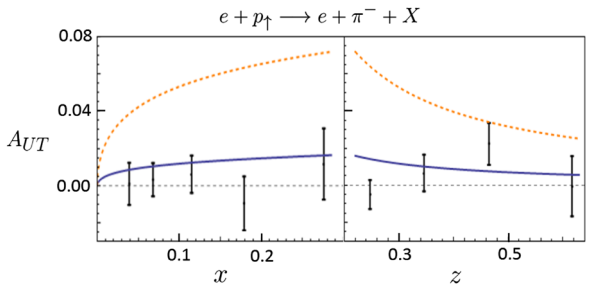

FIG. 5 (color online). Transversely polarized spin asymmetry [16] for π^- production. Q^2 is parametrized as $\sqrt{\langle Q^2\rangle} = 2.7408\langle x\rangle^{0.2793}$ ($R^2 = 0.9878$) [27] for the left graph, and $\langle Q^2\rangle = 2.41\ \text{GeV}^2$ [16] for the right graph. Our result (solid line) and the result in [14] (dashed line).

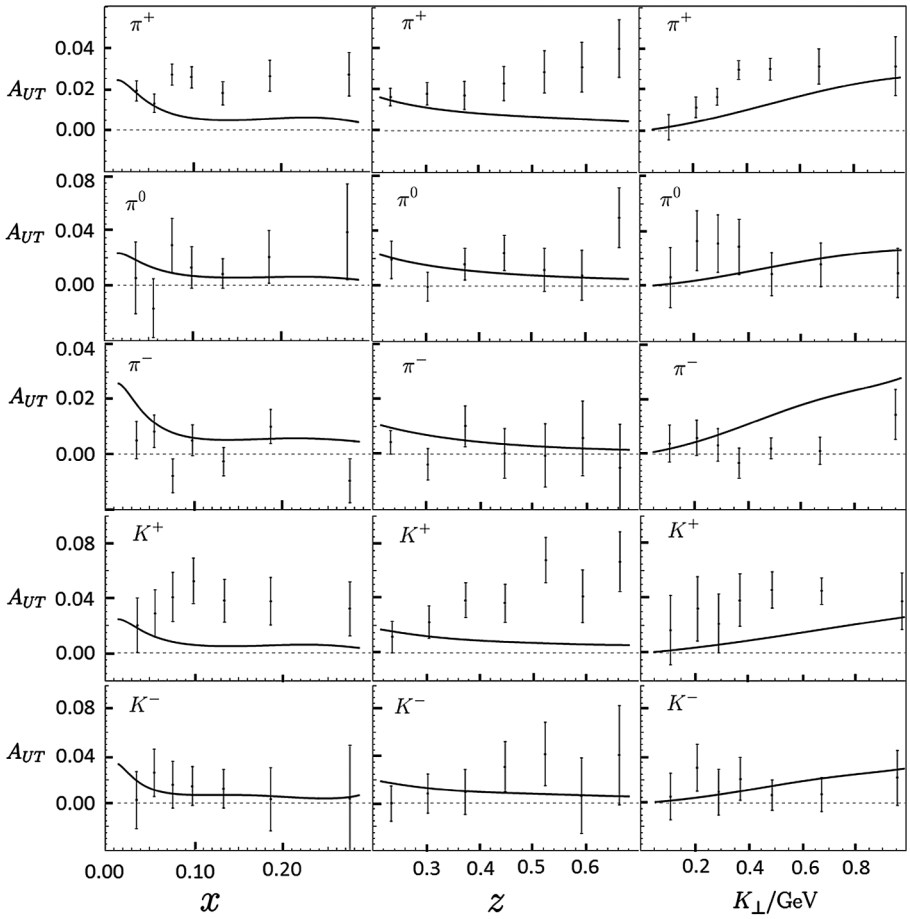

FIG. 6. Transversely polarized spin asymmetry (solid line) versus data [17].

longitudinal spin asymmetry (12) versus the data. The dashed line is the result in [14]. The differences stem from corrections to the analysis in [14].

The kinematical ranges for the transversely polarized HERMES experiment [16] are: $\langle x\rangle = 0.09$, $\langle y\rangle = 0.54$, $\langle z\rangle = 0.36$, $\langle K_\perp\rangle = 0.41$ GeV, and $\langle Q^2\rangle = 2.41$ GeV^2. In Fig. 5 we show our results (solid line) for the transversely polarized spin asymmetry (13) versus data. Our results correct minimally those reported in [14]. The one instanton contribution to the spin asymmetry is in good overall agreement with HERMES.

A better comparison with the data can be made using the recently reported HERMES results [17]. While the use of the average kinematics above is well motivated, a direct probing of the dependence of the transverse spin asymmetry on x, z, $K_\perp$ is even better. For instance, take the x dependent asymmetry of π^- with the empirical parametrizations to fit the reported kinematics from HERMES [17]: $\langle y\rangle = -95.737x^3 + 52.459x^2 - 9.0816x + 0.9495$, $\langle z\rangle = 15.67x^3 - 8.8459x^2 + 1.5193x + 0.2884$, $\langle K_\perp\rangle = 665.15x^4 - 444.02x^3 + 105.99x^2 - 10.843x + 0.7502$ (GeV), and $\langle Q^2\rangle = 20.371x + 0.4998$ (GeV^2). R^2 is above 0.97 for all the parametrizations. In Fig. 6 we compare our results (solid line) for the transverse polarization to the recent data [17]. The instanton induced asymmetry is in overall agreement for all π^+, π^0, π^-, K^+, and K^- production.

III. $P_\uparrow P$ COLLISION

The instanton mechanism used to generate T-odd amplitudes in SIDIS as detailed in Sec. II can be extended to $p_\uparrow p$ collision. In the center of mass (CM) frame the target proton is transversely polarized, while the projectile proton is unpolarized. As we are interested in the Sivers effect arising from a hard scattering process, we will only consider one instanton insertion tagged to a single gluon exchange. The π^+ productions are displayed in Figs. 7 and 8. The valence quark from the polarized proton exchanges one gluon with the valence quark from the unpolarized proton. The outgoing up quark with momentum k turns to the forward π^+.

Throughout, the proton will be viewed as 3 constitutive quarks with the gluons omitted. This simplified partonic description is motivated by the enhanced role played by the quark zero modes in the instanton background, and will help parallel the polarized SIDIS analysis with the inclusive hadron production in polarized $p_\uparrow p$. The translation from partonic to hadronic results will follow the SIDIS

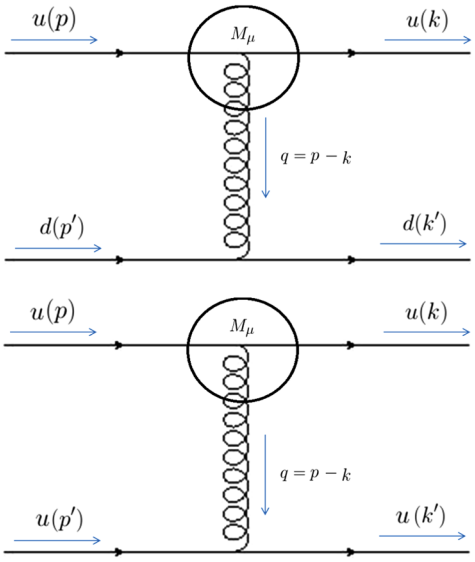

FIG. 7 (color online). The up quark from the transversely polarized proton and the quark from the unpolarized proton exchanges one gluon in the single instanton background (t-channel).

analysis. The inclusion of constitutive gluons will be addressed elsewhere.

The cross section arising from the process in Fig. 7 reads

$$d\sigma \sim \sum_{\text{color}} \frac{1}{q^4}\,\text{tr}[\not{k} M_{\mu,a} \not{p}(1+\gamma_5 \not{s}) M_{\nu,b}]\text{tr}[\not{k}' M^{\mu,a} \not{p}' M^{\nu,b}]. \tag{16}$$

As we are only interested in the spin dependent asymmetry, the overall coefficients in (16) will not be needed. Similarly to SIDIS, we set

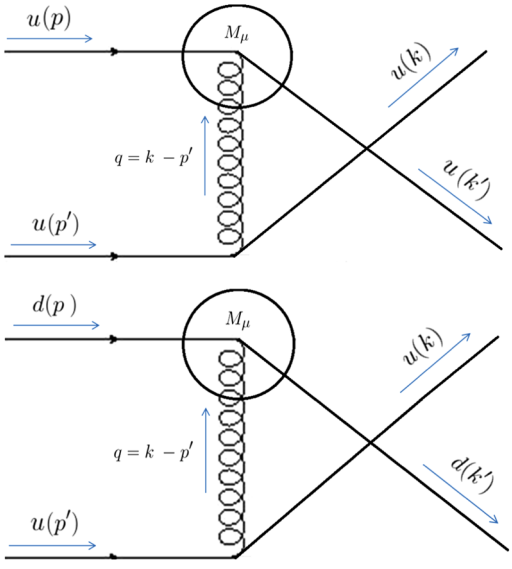

FIG. 8 (color online). The quark from the transversely polarized proton and the up quark from the unpolarized proton exchanges one gluon in the single instanton background (u-channel).

$$M_{\mu,a} = i g_s(\gamma_\mu t_a + M^{(1)}_{\mu,a}) \tag{17}$$

with the Gell-Mann color matrix t_a satisfying $\text{tr}[t_a t_b] = \frac{1}{2}\delta_{ab}$. After a short algebra we have

$$\begin{aligned} d^{(1)}\sigma &\sim \frac{g_s^4}{q^4}\sum_{\text{color}} \text{tr}[(M^{(1)}_{\mu,a} t_b \delta^{ab})\not{p}\gamma_5 \not{s}\gamma_\nu \not{k}]\text{tr}[\gamma^\mu \not{p}'\gamma^\nu \not{k}'], \\ d^{(0)}\sigma &\sim 2\frac{g_s^4}{q^4}\,\text{tr}[\gamma_\mu \not{p}\gamma_\nu \not{k}]\text{tr}[\gamma^\mu \not{p}'\gamma^\nu \not{k}']. \end{aligned} \tag{18}$$

In Appendix B we detail the calculation for the instanton induced vertex. In short

$$\sum_{\text{color}} M^{(1)}_{\mu,a} t_b \delta^{ab} = -i(\gamma_\mu \not{k} + \not{p}\gamma_\mu)\Psi(\rho|q|) \tag{19}$$

with

$$\Psi(a) \equiv \frac{2\pi^2\rho^4}{\lambda a^2}\left[\frac{4}{a^2} - \frac{4}{3}aK_1(a) - 2K_2(a) + \frac{1}{3}\right], \tag{20}$$

where again ρ is the instanton size and λ the mean quark zero mode virtuality.

We note that the sign of the vertex in (4) is opposite to that of the sign in (19). This sign flip explains the mismatch noted in [28] between the direction of azimuthal angles in SIDIS and $p_1 p$ collisions. It is reassuring that the nonperturbative instanton mechanism followed here is able to account for this flip which is apparently challenging in the perturbative framework.

After inserting (19) in (18), and using momentum conservation $k' = p' + p - k$ and $q = p - k$, we have

$$\begin{aligned} d^{(1)}\sigma &\sim 2^6 \frac{g_s^4}{|p-k|^4}[p'\cdot(k+p)\epsilon_{a\nu bc} s^a k^b p^c (p')^\nu] \\ &\quad \times \Psi(\rho|p-k|), \\ d^{(0)}\sigma &\sim 2^6 \frac{g_s^4}{|p-k|^4}\{2(k\cdot p')(p\cdot p') + (k\cdot p)[p'\cdot(p-k)]\}. \end{aligned}$$

Using the kinematical substitution,

$$p \to x_1 P_1, \qquad p' \to x_2 P_2, \qquad k' \to \frac{K}{z}, \tag{21}$$

we obtain

$$\begin{aligned} d^{(1)}\sigma &\sim 2^4 z g_s^4 \epsilon_{a\nu bc} S^a K^b P_1^c P_2^\nu G(x_1, x_2, x_F), \\ d^{(0)}\sigma &\sim 2^4 z g_s^4 H(x_1, x_2, x_F) \end{aligned} \tag{22}$$

with

$$\begin{aligned} G(x_1, x_2, x_F) &\equiv \frac{x_2}{x_1}\frac{1}{(K\cdot P_1)^2}\Psi\left(\rho\sqrt{\frac{2x_1}{z}K\cdot P_1}\right) \\ &\quad \times\left[x_2 P_2\cdot\left(\frac{K}{z} + x_1 P_1\right)\right], \end{aligned} \tag{23}$$

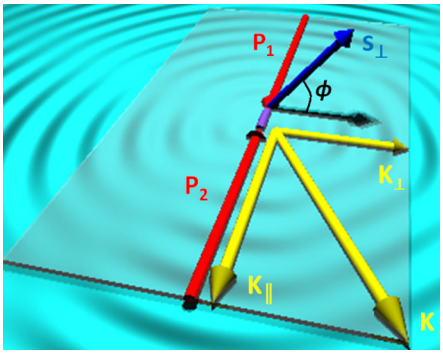

FIG. 9 (color online). Two protons moving head-on in the CM frame. The two protons and the outgoing pion are in the same plane. The angle between the transversely polarized spin $S_\perp$ and this plane is ϕ. The convention for azimuthal angle is consistent with experiments.

$$H(x_1,x_2,x_F) \equiv \frac{x_2}{x_1}\frac{2x_2(K\cdot P_2)(P_1\cdot P_2)+(K\cdot P_1)[P_2\cdot(x_1P_1-\frac{K}{z})]}{(K\cdot P_1)^2}. \tag{24}$$

The kinematics of the collision process $p_\uparrow p$ is shown in Fig. 9.

The contribution $\epsilon_{\alpha\nu bc}S^aK^bP_1^cP_2^\nu$ in (22) yields the $\sin\phi$ behavior of the asymmetry in $p_\uparrow p$ (Sivers effect)

$$\epsilon_{\alpha\nu bc}S^aK^bP_1^cP_2^\nu = \frac{s}{2}K_\perp S_\perp \sin\phi, \tag{25}$$

where $s=(P_1+P_2)^2$, $K_\perp$ is the transverse momentum of the outgoing pion, and $S_\perp$ is transverse spin. In the CM frame, $P_1=\sqrt{s}/2(1,0,0,1)$, $P_2=\sqrt{s}/2(1,0,0,-1)$, and $K=(E,K_\perp,0,x_F\sqrt{s}/2)$, where x_F is the pion longitudinal momentum fraction ($K_\parallel=x_F\sqrt{s}/2$), and $E=\sqrt{M_\pi^2+K_\perp^2+(x_F\sqrt{s}/2)^2}$ is the pion energy. $x_F>0$ stands for forward pion production, while $x_F<0$ stands for backward pion production.

Combining the above results, yields

$$\begin{aligned} d^{(1)}\sigma &\sim 2^4 z g_s^4 \frac{s}{2}K_\perp S_\perp \sin\phi G(x_1,x_2,x_F),\\ d^{(0)}\sigma &\sim 2^4 z g_s^4 H(x_1,x_2,x_F), \end{aligned} \tag{26}$$

where

$$G(x_1,x_2,x_F)=\frac{x_2}{x_1}\frac{\Psi(\rho\sqrt{\frac{\sqrt{s}x_1}{z}(E-x_F\frac{\sqrt{s}}{2})})}{[\frac{\sqrt{s}}{2}(E-x_F\frac{\sqrt{s}}{2})]^2} \times\left\{\frac{x_2}{z}\left[\frac{\sqrt{s}}{2}\left(E+x_F\frac{\sqrt{s}}{2}\right)\right]+x_1x_2\frac{s}{2}\right\}, \tag{27}$$

$$H(x_1,x_2,x_F)=\frac{\frac{x_2}{x_1}}{\left[\frac{\sqrt{s}}{2}(E-x_F\frac{\sqrt{s}}{2})\right]^2} \times\left\{\frac{x_2 s^{(3/2)}}{2}\left(E+x_F\frac{\sqrt{s}}{2}\right)+\frac{\sqrt{s}}{2}\left(E-x_F\frac{\sqrt{s}}{2}\right) \times\left[x_1\frac{s}{2}-\frac{\sqrt{s}}{2z}\left(E+x_F\frac{\sqrt{s}}{2}\right)\right]\right\}. \tag{28}$$

A rerun of the above analysis for the cross section arising from the process in Fig. 8 yields

$$\begin{aligned} d^{(1)}\sigma &\sim -2^4 z g_s^4 \frac{s}{2}K_\perp S_\perp \sin\phi G(x_2,x_1,-x_F),\\ d^{(0)}\sigma &\sim 2^4 z g_s^4 H(x_2,x_1,-x_F). \end{aligned} \tag{29}$$

We set $S_\perp u(x,Q^2)=\Delta u_s(x,Q^2)/2$ and $S_\perp d(x,Q^2)=\Delta d_s(x,Q^2)/2$, with $\Delta u_s(x,Q^2)$ and $\Delta d_s(x,Q^2)$ as the spin polarized distribution functions of the valence up quarks and valence down quarks in the proton, respectively. For simplicity, we denote $g(x)\equiv\Delta u_s(x,Q^2)/u(x,Q^2)$, $h(x)\equiv\Delta d_s(x,Q^2)/d(x,Q^2)$, and $R(x)=1/r(x)\equiv d(x,Q^2)/u(x,Q^2)$. Thus, the respective SSAs for π^+, π^-, and π^0 follow in the form

$$A_{TU}^{\sin\phi}(\pi^+)=\frac{s}{4}K_\perp\frac{g(x_1)[1+R(x_2)]G(x_1,x_2,x_F)-[g(x_1)+h(x_1)R(x_1)]G(x_2,x_1,-x_F)}{[1+R(x_2)]H(x_1,x_2,x_F)+[1+R(x_1)]H(x_2,x_1,-x_F)}, \tag{30}$$

$$A_{TU}^{\sin\phi}(\pi^-)=\frac{s}{4}K_\perp\frac{h(x_1)[1+r(x_2)]G(x_1,x_2,x_F)-[h(x_1)+g(x_1)r(x_1)]G(x_2,x_1,-x_F)}{[1+r(x_2)]H(x_1,x_2,x_F)+[1+r(x_1)]H(x_2,x_1,-x_F)}, \tag{31}$$

$$A_{TU}^{\sin\phi}(\pi^0)=\frac{s}{4}K_\perp\frac{g(x_1)+R(x_1)h(x_1)}{1+R(x_1)}\frac{G(x_1,x_2,x_F)-G(x_2,x_1,-x_F)}{H(x_1,x_2,x_F)+H(x_2,x_1,-x_F)}. \tag{32}$$

The asymmetries in (30)–(32) are proportional to $\sin\phi$. We note that for a wide range of $x_{1,2}$ i.e. between (0.01–0.99), $A_{TU}^{\sin\phi}(\pi^+)$ and $A_{TU}^{\sin\phi}(\pi^0)$ are positive while $A_{TU}^{\sin\phi}(\pi^-)$ is negative. As the transverse momentum $K_\perp$ increases, the asymmetries in (30)–(32) vanish due to the modified Bessel function in the formula. To compare with the PHENIX experiment [20], we assume the mean factorization $\langle x_1\rangle=\langle x_2\rangle=0.5$, $\langle z\rangle=0.5$, and $\langle x_F\rangle=0.3$. We have reset the mean instanton quark zero mode virtuality $\bar{\lambda}\approx 1/(0.2\,\text{GeV})^3$ and instanton size $\rho\approx 0.43$ fm. The averaged transverse momentum of the outgoing π^0 is $\langle K_\perp\rangle=1$ GeV. According to [29,30], $g(x)=0.959-0.588(1-x^{1.048})$,

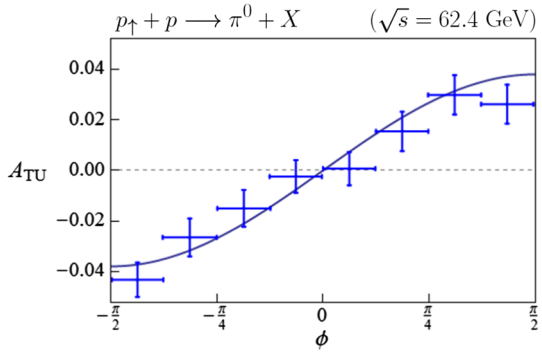

FIG. 10 (color online). ϕ dependent SSA in $p_\uparrow p$ collision at $\sqrt{s} = 62.4$ GeV [20]. Our result is the solid line.

$h(x) = -0.773 + 0.478(1 - x^{1.243})$, and $R(x) = 1/r(x) = 0.624(1 - x)$. In Fig. 10 we show our results (solid line) versus the PHENIX data [20].

A more thorough comparison to the wide range of kinematics swept by PHENIX and STAR $\sqrt{s} \approx$ (19.4–200) GeV is displayed in Figs. 11–13. For simplicity, we set the parameters $\langle x_1 \rangle = \langle x_2 \rangle = 0.5$ and $\langle z \rangle = 0.5$ at their mean value. The instanton size is $\rho \approx 0.72$ fm at $\sqrt{s} = 19.4$ GeV, $\rho \approx 0.43$ fm at $\sqrt{s} = 62.4$ GeV, and $\rho \approx 0.65$ fm at $\sqrt{s} = 200$ GeV. Instanton size fluctuations are present in the QCD vacuum. The averaged outgoing momentum of mesons is $\langle K_\perp \rangle = 1$ GeV at $\sqrt{s} = 19.4$ GeV [22]; $\langle K_\perp \rangle = 0.9$ GeV for $\eta < 3.5$ and $\langle K_\perp \rangle = 0.4$ GeV for $\eta > 3.5$ at $\sqrt{s} = 62.4$ GeV [21]; $\langle K_\perp \rangle = 2$ GeV for $\eta < 3.5$; and $\langle K_\perp \rangle = 1.5$ GeV for $\eta > 3.5$ at $\sqrt{s} = 200$ GeV [19].

Recently, the SSA in backward π^0 production has been measured by the STAR Collaboration [19]. To compare our results with the data for both forward π^0 productions and backward π^0 productions, we need to improve on the mean factorization approximation we used with $\langle x_1 \rangle = \langle x_2 \rangle = 0.5$. This can be done by noting that in forward π^0 production (positive $\langle x_F \rangle$) a smaller $\langle x_F \rangle$ (compared to

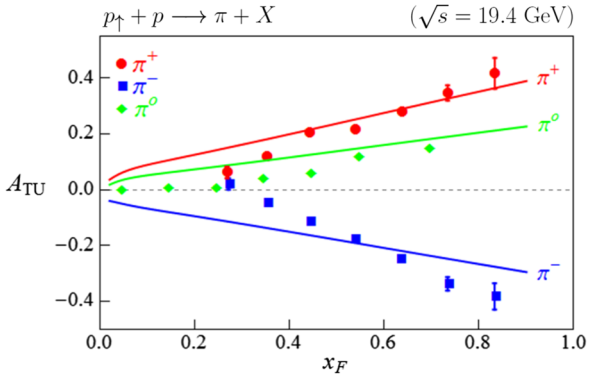

FIG. 11 (color online). x_F dependent transversely polarized spin asymmetry in $p_\uparrow p$ collision at $\sqrt{s} = 19.4$ GeV [22]. The averaged outgoing momentum of the pions is $\langle K_\perp \rangle = 1$ GeV. The red (π^+), blue (π^-), and green (π^0) solid lines stand for the SSA in π^+ (30), π^- (31), and π^0 (32) productions respectively.

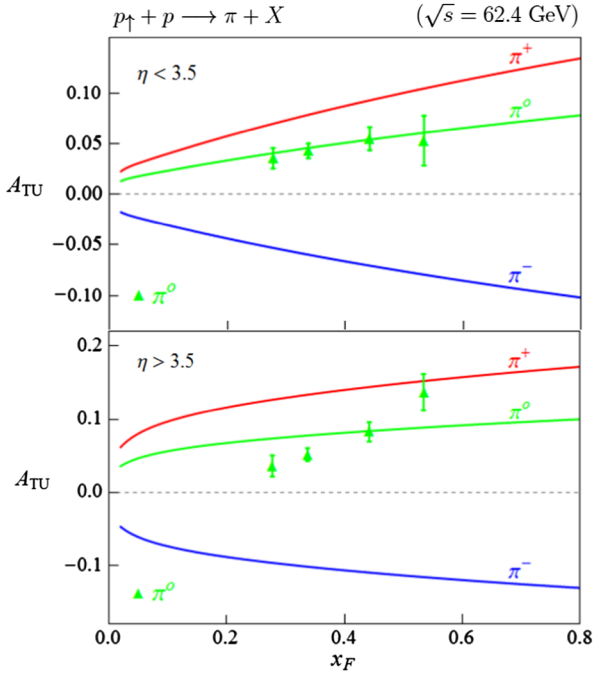

FIG. 12 (color online). x_F dependent transversely polarized spin asymmetry in $p_\uparrow p$ collision at $\sqrt{s} = 62.4$ GeV [21]. The averaged outgoing momentum of π^0 is $\langle K_\perp \rangle = 0.9$ GeV for $\eta < 3.5$ and $\langle K_\perp \rangle = 0.4$ GeV for $\eta > 3.5$. The red (π^+), blue (π^-), and green (π^0) solid lines stand for the SSA in π^+ (30), π^- (31), and π^0 (32) productions, respectively.

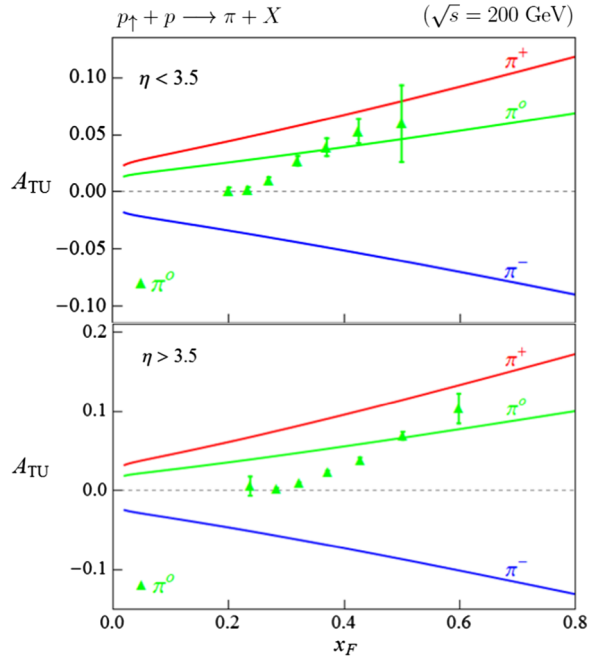

FIG. 13 (color online). x_F dependent transversely polarized spin asymmetry in $p_\uparrow p$ collision at $\sqrt{s} = 200$ GeV [19]. The averaged outgoing momentum of π^0 is $\langle K_\perp \rangle = 2$ GeV for $\eta < 3.5$ and $\langle K_\perp \rangle = 1.5$ GeV for $\eta > 3.5$. The red (π^+), blue (π^-), and green (π^0) solid lines stand for the SSA in π^+ (30), π^- (31), and π^0 (32) productions, respectively.

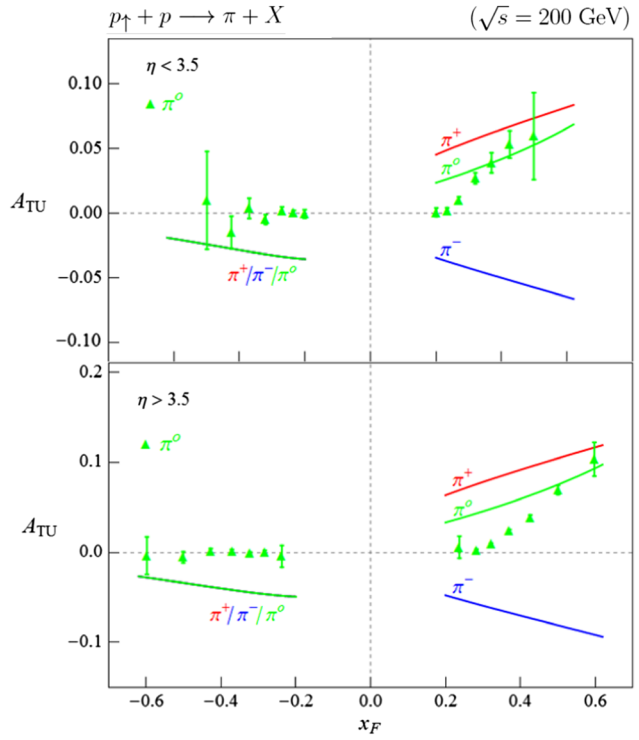

FIG. 14 (color online). x_F dependent transversely polarized spin asymmetry in $p_\uparrow p$ collision at $\sqrt{s} = 200$ GeV [19]. The averaged outgoing momentum of π^0 is $\langle K_\perp \rangle = 2$ GeV for $\eta < 3.5$ and $\langle K_\perp \rangle = 1.5$ GeV for $\eta > 3.5$. Positive x_f is forward π^0 productions. Negative x_f is backward π^0 productions. The red (π^+), blue (π^-), and green (π^0) solid lines stand for the SSA in π^+ (30), π^- (31), and π^0 (32) productions, respectively. For backward pion productions ($x_F < 0$), the SSAs in π^+ (30), π^- (31), and π^0 (32) productions coincide.

the mean factorization value of 0.5), implies that $\langle x_2 \rangle \uparrow$ and $\langle x_1 \rangle \downarrow$. In contrast, a larger $\langle x_F \rangle$ (compared to the mean factorization value of 0.5), would imply $\langle x_2 \rangle \downarrow$ and $\langle x_1 \rangle \uparrow$. The same analysis reveals that $\langle x_1 \rangle$ and $\langle x_2 \rangle$ behaves oppositely for negative $\langle x_F \rangle$. Therefore, we choose to parametrize the values of $\langle x_1 \rangle$ and $\langle x_2 \rangle$ as follows: for positive $\langle x_F \rangle$, $\langle x_1 \rangle = \langle x_F \rangle + 0.2$ and $\langle x_2 \rangle = 0.8 - \langle x_F \rangle$; for negative $\langle x_F \rangle$: $\langle x_2 \rangle = \langle x_F \rangle + 0.2$ and $\langle x_1 \rangle = 0.8 - \langle x_F \rangle$. The comparison is displayed in Fig. 14. Remarkably, all backward pion productions whether charged or uncharged coincide, despite the many differences in the kinematical details. This feature follows from large $\sqrt{s}$ as we now detail.

In the large $\sqrt{s}$ limit, the SSAs for the three forward pion productions ($x_F > 0$) simplify as only the t-channel process dominates. Specifically

$$A_{TU}^{\sin\phi}(\pi^+) \approx g(x_1) \frac{K_\perp}{4z} \Psi\left(\rho \frac{K_\perp}{z} \sqrt{\frac{x_1 z}{x_F}}\right)\left(1 + \frac{x_1 z}{x_F}\right), \tag{33}$$

$$A_{TU}^{\sin\phi}(\pi^-) \approx h(x_1) \frac{K_\perp}{4z} \Psi\left(\rho \frac{K_\perp}{z} \sqrt{\frac{x_1 z}{x_F}}\right)\left(1 + \frac{x_1 z}{x_F}\right), \tag{34}$$

$$A_{TU}^{\sin\phi}(\pi^0) \approx \frac{g(x_1) + h(x_1)R(x_1)}{1 + R(x_1)} \frac{K_\perp}{4z} \times \Psi\left(\rho \frac{K_\perp}{z} \sqrt{\frac{x_1 z}{x_F}}\right)\left(1 + \frac{x_1 z}{x_F}\right). \tag{35}$$

For the backward pion productions ($x_F < 0$), the u-channel process dominates leading to

$$A_{TU}^{\sin\phi}(\pi^+) = A_{TU}^{\sin\phi}(\pi^-) = A_{TU}^{\sin\phi}(\pi^0) = -\frac{g(x_1) + h(x_1)R(x_1)}{1 + R(x_1)} \frac{K_\perp}{4z} \times \Psi\left(\rho \frac{K_\perp}{z} \sqrt{\frac{x_2 z}{|x_F|}}\right)\left(1 + \frac{x_2 z}{|x_F|}\right). \tag{36}$$

For completeness, we recall that

$$g(x_1) = \frac{\Delta u_s(x_1, Q^2)}{u(x_1, Q^2)}, \quad h(x_1) = \frac{\Delta d_s(x_1, Q^2)}{d(x_1, Q^2)}, \quad \frac{g(x_1) + h(x_1)R(x_1)}{1 + R(x_1)} = \frac{\Delta u_s(x_1, Q^2) + \Delta d_s(x_1, Q^2)}{u(x_1, Q^2) + d(x_1, Q^2)}. \tag{37}$$

For $\sqrt{s} > 100$ GeV the deviation of (33)–(36) from their nonasymptotic values is less than 1%. At large $\sqrt{s}$ the SSA in $p_\uparrow p$ following from the one-instanton insertion is generic. All SSAs for backward pion productions (36) coincide as we show in Fig. 14. In Fig. 15 we display our predictions for the SSA for forward pion production at $\sqrt{s} = 500$ GeV which is expected to be measured by the STAR Collaboration. Since our results depend on the mean value of the transverse pion momentum $\langle K_\perp \rangle$ and the size of the instanton $\langle \rho \rangle$, Fig. 15 displays a reasonable choice range. We recall that the instanton's size fluctuates in the vacuum. Overall, our predictions are robust against this reasonable change in the parameters.

IV. CONCLUSIONS

We have suggested that QCD instantons may contribute significantly to the longitudinal and transverse SSA in SIDIS. The diluteness of the QCD instantons in the vacuum justifies the use of the single instanton approximation. Our analysis and results are in reasonable agreement for most of the measured pion and kaon production channels. The same mechanism when applied to $p_\uparrow p$ collisions, provides a natural explanation for the Sivers contribution. Our results are in agreement with the reported data in a wide range of $\sqrt{s} = 19.4$–200 GeV. Remarkably, the sign in our result is in agreement with the experiments both in SIDIS and $p_\uparrow p$ collisions. We have predicted the SSA for forward charged pion productions, and backward both charged and uncharged pion productions for a wide range of collider

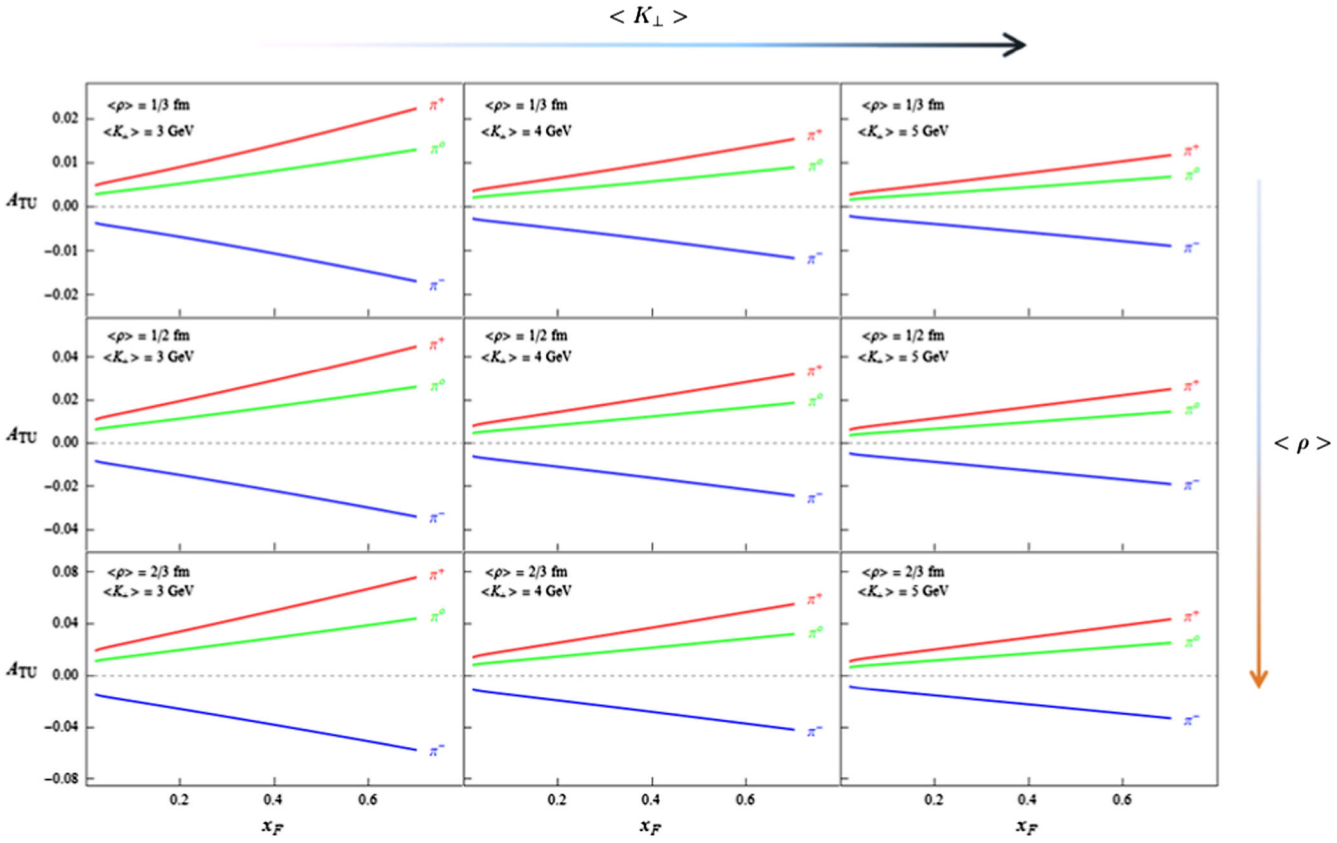

FIG. 15 (color online). Expected x_F dependence of the SSA in forward pion production in $p_\uparrow p$ collision at $\sqrt{s} = 500$ GeV.

energies. All backward productions coincide irrespective of the differences in their kinematics at large $\sqrt{s}$.

ACKNOWLEDGMENTS

This work was supported in parts by the U.S. DOE Grant No. DE-FG-88ER40388.

APPENDIX A: PHOTON EXCHANGE

In this Appendix, we provide the detail derivation of (4), corresponding to the nonperturbative insertion $M_\mu^{(1)}$ for photon exchange in the single instanton background. The calculation here is similar to [14,26]. According to [14,26,31,32], the zero mode quark propagator in the single instanton background after Fourier transformation with respect to the incoming momentum p is

$$S_0(x,p)_{\dot\beta}{}^{j}{}_{i\delta} = \frac{2\rho^2}{\lambda}\frac{x^l(\bar\sigma_l)_{\dot\beta\gamma}\varepsilon^{\gamma j}\varepsilon_{i\delta}}{(x^2+\rho^2)^{(3/2)}|x|}. \tag{A1}$$

Note the chirality of the zero mode flips as $|L\rangle\langle R|$ as depicted in Fig. 16. The incoming quark is left-handed and has momentum p (on-shell). ρ is the size of instanton and λ is the mean virtuality. β and δ are spatial indices, while j and i are color indices. In Euclidean space, $\sigma_\mu = (\vec\sigma, iI)$, $\bar\sigma_\mu = (\vec\sigma, iI)$, and $\epsilon^{01} = -\epsilon^{10} = -\epsilon_{01} = \epsilon_{10}$ [33].

The right-handed nonzero mode quark propagator in the single instanton after Fourier transformation with respect to the outgoing momentum k is [14,26,31]

$$S_{nz}(k,x)^{\beta i}{}_{j\alpha} = -\left[\delta^i_j + \frac{\rho^2}{x^2}\frac{(\sigma_\rho\bar\sigma_r)^i{}_j k^\rho x^r}{2k\cdot x}(1-e^{-ik\cdot x})\right] \times \frac{|x|}{\sqrt{x^2+\rho^2}}e^{ik\cdot x}\delta^\beta_\alpha. \tag{A2}$$

As the instanton size approaches zero ($\rho \to 0$) or the instanton is far away ($x_0 \to \infty$), the nonzero mode propagator becomes the free propagator. This point will be revisited later.

Consider the process depicted in Fig. 16: The incoming left-handed quark meets one instanton and flips its chirality (zero mode), then exchanges one photon, and finally becomes an outgoing right-handed quark. As a result, the nonperturbative insertion $M_\mu^{(1)}$ reads

$$(M_\mu^{(1)})^{\beta i}{}_{i'\delta} = \int d^4x e^{-iq\cdot x} S_{nz}(k,x)^{\beta i}{}_{j\alpha}\sigma_\mu^{\alpha\dot\beta} S_0(x,p)_{\dot\beta}{}^{j}{}_{i'\delta}. \tag{A3}$$

All the other parts of the diagram are trivial in color, therefore we take the trace of color indices i and i'. To further simplify the result, we need the following formula [33]:

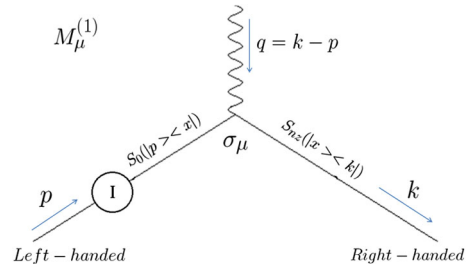

FIG. 16 (color online). The incoming left-handed quark with momentum p meets one instanton and flips its chirality. The outgoing right-handed quark carries momentum k. The momentum of the photon is $q = p - k$. S_0 and S_{nz} stand for the zero mode quark propagator and the nonzero mode quark propagator in the single instanton background, respectively.

$$\delta_\alpha^\beta \delta_j^i (\sigma_\mu)^{\alpha\dot\beta}(\bar\sigma_l)_{\dot\beta\gamma}\varepsilon^{\gamma j}\varepsilon_{i\delta} = (\sigma_\mu\bar\sigma_l)^\beta{}_\delta, \tag{A4}$$

$$\delta_\alpha^\beta (\sigma_\rho\bar\sigma_r)^i{}_j (\sigma_\mu)^{\alpha\dot\beta}(\bar\sigma_l)_{\dot\beta\gamma}\varepsilon^{\gamma j}\varepsilon_{i\delta} = (\sigma_\mu\bar\sigma_l\sigma_r\bar\sigma_\rho)^\beta{}_\delta. \tag{A5}$$

Combining all the equations above, we obtain

$$M_\mu^{(1)} = -\int d^4x \Big[\frac{2\rho^2}{\lambda}\sigma_\mu\bar\sigma_l e^{ip\cdot x}\frac{x^l}{(x^2+\rho^2)^2} + \sigma_\mu\bar\sigma_\rho k^\rho \frac{\rho^4}{\lambda}(e^{ip\cdot x} - e^{-iq\cdot x})\frac{1}{(x^2+\rho^2)^2(k\cdot x)}\Big]. \tag{A6}$$

The d^4x integration in (A6) can be done with the help of the following formula ($p^2 \to 0$):

$$\int d^4x e^{ip\cdot x}\frac{x^l}{(x^2+\rho^2)^2} = i2\pi^2\frac{p^l}{p^2}, \tag{A7}$$

$$\int d^4x \frac{e^{ip\cdot x}}{(x^2+\rho^2)^2(k\cdot x)} = -i\frac{2\pi^2}{p\cdot k}\frac{\rho|p|}{\rho^2}K_1(\rho|p|) = i\frac{4\pi^2}{q^2}\frac{\rho|p|}{\rho^2}K_1(\rho|p|), \tag{A8}$$

where we used $-2p\cdot k = (k-p)^2 - k^2 - p^2 \approx q^2$. The denominator in (A7) appears to diverge as $p^2 \to 0$. We show below that all terms proportional to $\bar\sigma_l p^l$ vanish.

Thus,

$$M_\mu^{(1)} = -i\frac{4\pi^2\rho^2}{\lambda}\sigma_\mu\bar\sigma_l\Big[\frac{k^l}{q^2}(f(\rho|p|) - f(\rho|q|)) + \frac{p^l}{p^2}\Big], \tag{A9}$$

where $f(a) = aK_1(a)$ As the incoming quark with momentum p is on-shell and the mass of the quark is small ($p^2 \to 0$), we have

$$f(\rho|p|) = \rho|p|K_1(\rho|p|) \to \rho|p|\frac{1}{\rho|p|} = 1. \tag{A10}$$

Since $q^2 < 0$ in SIDIS, we define $Q^2 = -q^2 > 0$. (A9) simplifies to

$$M_\mu^{(1)} = i\frac{4\pi^2\rho^2}{\lambda}\sigma_\mu\bar\sigma_l\Big[\frac{k^l}{Q^2}(1 - f(\rho Q)) - \frac{p^l}{p^2}\Big]. \tag{A11}$$

If we consider that the incomging right-handed quark flips its spin and becomes left-handed one, we only need to conjugate (A11) and substitute $k \leftrightarrow -p$

$$M_\mu^{(1)} = i\frac{4\pi^2\rho^2}{\lambda}(\sigma_\mu\bar\sigma_l k^l + \sigma_l\bar\sigma_\mu p^l)\frac{1}{Q^2}(1 - f(\rho Q)) - i\frac{4\pi^2\rho^2}{\lambda}\Big(\sigma_\mu\bar\sigma_l\frac{p^l}{p^2} + \sigma_l\bar\sigma_\mu\frac{k^l}{k^2}\Big). \tag{A12}$$

If the anti-instanton is also included ($\sigma \leftrightarrow \bar\sigma$), we have the compact form

$$M_\mu^{(1)} = i\frac{4\pi^2\rho^2}{\lambda Q^2}[\gamma_\mu \not{k} + \not{p}\gamma_\mu](1 - f(\rho Q)) - i\frac{4\pi^2\rho^2}{\lambda}\Big[\gamma_\mu\frac{\not{p}}{p^2} + \gamma_\mu\frac{\not{k}}{k^2}\Big]. \tag{A13}$$

The last two terms in (A13) vanish. Indeed, set $\gamma_\mu\not{p}/p^2$ and insert it in the hadronic tensor $W_{\mu\nu}$ (2). Thus,

$$\lim_{p^2\to 0}\mathrm{tr}\Big[\gamma_\mu\frac{\not{p}}{p^2}\not{p}\gamma_5\not{s}\gamma_\nu\not{k}\Big] = \mathrm{tr}[\gamma_\mu\gamma_5\not{s}\gamma_\nu\not{k}], \tag{A14}$$

where the indices μ and ν are antisymmetric. The same indices are symmetric in the leptonic tensor (1). Thus the two contract to zero.

Finally, we explicitly show that all terms proportional to $\bar\sigma_l p^l$ in (A9) vanish. For that, rewrite (A2) as

$$S_{nz}(k,x) = -\frac{\rho^2}{x^2}\frac{(\sigma_\rho\bar\sigma_r)^i{}_j k^\rho x^r}{2k\cdot x}\frac{(1 - e^{-ik\cdot x})|x|}{\sqrt{x^2+\rho^2}}e^{ik\cdot x}\delta_\alpha^\beta - \frac{|x|}{\sqrt{x^2+\rho^2}}e^{ik\cdot x}\delta_\alpha^\beta\delta_j^i. \tag{A15}$$

As the instanton size $\rho \to 0$, the first contribution in (A15) vanishes and the second contribution reduces to the free propagator. As a result, the chirality flip vertex $M_\mu^{(1)}$ vanishes. The second contribution in (A15) is at the origin of the term proportional $\bar\sigma_l p^l$. This analysis is general and will be exported to the gluon vertex below.

To summarize, the instanton vertex to be used following a photon insertion is

$$M_\mu^{(1)} = i\frac{4\pi^2\rho^2}{\lambda Q^2}[\gamma_\mu\not{k} + \not{p}\gamma_\mu](1 - f(\rho Q)), \tag{A16}$$

which is (4).

APPENDIX B: GLUON EXCHANGE

In this Appendix we derive (19), corresponding to the nonperturbative insertion $M_\mu^{(1)}$ for gluon exchange in the single instanton background. The calculation is similar to the photon exchange (see Appendix A). Consider the following case: The

incoming left-handed quark with momentum p flips its chirality (zero mode), exchange one gluon, and finally becomes the right-handed outgoing quark with momentum k in the single instanton background as depicted in Fig. 17.

This diagram is similar to the photon exchange one, but now the gluon carries color. Since the instanton is SU(2) valued, we embed the SU(2) in the upper corner of SU(3) to perform the color tracing. Thus,

$$S_0(x,p)_{\dot\beta}{}^{j}{}_{i\delta} = \begin{cases} \frac{2\rho^2}{\lambda}\frac{x^l(\bar\sigma_l)_{\dot\beta\gamma}\varepsilon^{\gamma j}\varepsilon_{i\delta}}{(x^2+\rho^2)^{(3/2)}|x|} & (i,j=1,2) \\ 0 & (j=3 \ \text{ or } \ i=3), \end{cases} \tag{B1}$$

where $S_0(x,p)$ is the zero mode quark propagator in the single instanton background after Fourier transforming with respect to the incoming particle momentum p.

$$S_{nz}(k,x)^{\beta i}{}_{j\alpha} = \begin{cases} -\frac{|x|}{\sqrt{x^2+\rho^2}} e^{ik\cdot x}\delta^\beta_\alpha\left[\delta^i_j + \frac{\rho^2}{x^2}\frac{(\sigma_\rho\bar\sigma_r)^i_j k^\rho x^r}{2k\cdot x}(1-e^{-ik\cdot x})\right] & (i,j=1,2) \\ -e^{ik\cdot x}\delta^\beta_\alpha\delta^i_j & (i=3), \end{cases} \tag{B2}$$

where $S_{nz}(k,x)$ is the right-handed nonzero mode quark propagator in the single instanton after Fourier transforming with respect to outgoing particle with momentum k.

The nonperturbative insertion $M^{(1)}$ in (18) is given by

$$M^{(1)a}{}_\mu = \int d^4x e^{iq\cdot x} S_{nz}(k,x)^{\beta i}{}_{j\alpha}\sigma_\mu^{\alpha\dot\beta}(t^a)^j{}_{j'}S_0(x,p)_{\dot\beta}{}^{j'}{}_{i'\delta}. \tag{B3}$$

Combining (B1)–(B3), we get (19). To keep the number of indices from mushrooming we need to recombine the expressions. The first observation is that the nonzero mode $S_{nz}(k,x)$ will become the free propagator if the instanton size $\rho\to 0$. Therefore, we first pick the terms with trial color indices in $S_{nz}(k,x)^{\beta i}{}_{j\alpha}$ (these contain δ^i_j). The contribution to the vertex of such terms is given by

$$-\frac{2\rho^2}{\lambda}\delta^{ab}\int d^4x e^{i(k+q)\cdot x}\frac{x^l(\sigma_\mu\bar\sigma_l\epsilon)^{\beta j'}}{(x^2+\rho^2)^{(3/2)}|x|} \times\left\{[t^T_a]_{j'}{}^{i=3}[t^T_b]_{i=3}{}^{i'} + \sum_{i=1,2}\frac{|x|}{\sqrt{x^2+\rho^2}}[t^T_a]_{j'}{}^{i}[t^T_b]_i{}^{i'}\right\}\epsilon_{i'\delta}. \tag{B4}$$

Since $k+q=p$ and $p^2\approx 0$, we can simplify (B4) into

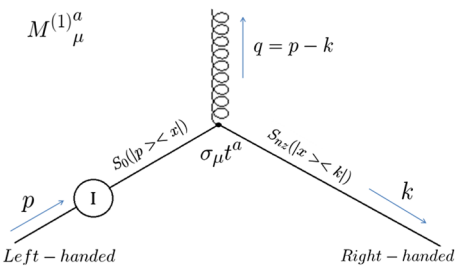

FIG. 17 (color online). The incoming left-handed quark with momentum p meets one instanton and flips its chirality. The outgoing right-handed quark carries momentum k. The momentum of the gluon is $q=k-p$. S_0 and S_{nz} stand for zero mode quark propagator and nonzero mode quark propagator in single instanton background, respectively.

$$-\frac{2\rho^2}{\lambda}\int d^4x\frac{e^{ip\cdot x}}{|x|}\frac{x^l(\sigma_\mu\bar\sigma_l\epsilon)^{\beta j'}}{(x^2+\rho^2)^{(3/2)}}\sum_{i=1,2,3}[t^T_a]_{j'}{}^{i}[t^a]^{Ti'}{}_{i}\epsilon_{i'\delta} = -\frac{8\rho^2}{3\lambda}(\sigma_\mu\bar\sigma_l)\int d^4x e^{ip\cdot x}\frac{x^l}{x^2}\to(\cdots)\bar\sigma_l p^l. \tag{B5}$$

As we discussed earlier, the terms proportional to $\bar\sigma_l p^l$ finally vanish (see Appendix A).

Collecting all the terms left, we have

$$-\frac{\rho^4}{\lambda}\delta^{ab}\int d^4x(e^{ip\cdot x}-e^{iq\cdot x})\frac{1}{(x^2+\rho^2)^2}\frac{1}{x^2}\frac{k^\rho x^r x^l}{k\cdot x} \times\left[\sum_{i=1,2}\sum_{j=1,2}(\sigma_\mu\bar\sigma_l\epsilon)^{\beta j'}[t^T_a]_{j'}{}^{j}[\sigma_\rho\bar\sigma_r]^T{}_j{}^{i}[t^T_b]_i{}^{i'}\epsilon_{i'\delta}\right]. \tag{B6}$$

Note that $\{i,j\}=\{1,2\}$ is due to our choice of the SU(2) instanton embedding into SU(3). The final result should not dependent on this embedding. Indeed, for an arbitrary SU(2) group element g, we expect

$$\sum_{i,j=\{1,2\}}\delta^{ab}[t^T_a]_{j'}{}^{j}g_j{}^{i}[t^T_b]_i{}^{i'} = \sum_{i,j=\{2,3\}}\delta^{ab}[t^T_a]_{j'}{}^{j}g_j{}^{i}[t^T_b]_i{}^{i'} = \sum_{i,j=\{3,1\}}\delta^{ab}[t^T_a]_{j'}{}^{j}g_j{}^{i}[t^T_b]_i{}^{i'}.$$

The coefficients are given by

$$\sum_{i,j=\{1,2\}}\delta^{ab}[t^T_a]_{j'}{}^{j}I_j{}^{i}[t^T_b]_i{}^{i'} = \frac{5}{6}I_{j'}{}^{i'}, \tag{B7}$$

$$\sum_{i,j=\{1,2\}}\delta^{ab}[t^T_a]_{j'}{}^{j}(\sigma_m)_j{}^{i}[t^T_b]_i{}^{i'} = -\frac{1}{6}(\sigma_m)_{j'}{}^{i'}. \tag{B8}$$

These two coefficients are different as the instaonton color indices are diagonal and couple with spin in a nontrivial way.

Inserting (B7) and (B8) in (B6), we obtain new terms. The d^4x integration can be done with the help of (A7) and (A8), and

$$\int d^4x e^{iq\cdot x}\frac{1}{(x^2+\rho^2)^2}\frac{x^l}{x^2} = i2\pi^2 q^l \frac{4-(\rho|q|)^3K_1(\rho|q|)-2(\rho|q|)^2K_2(\rho|q|)}{(\rho|q|)^4}. \tag{B9}$$

Combining the previous results, substituting $q = p - k$ and $|q| = \sqrt{2p\cdot k}$, and dropping all the terms proportional to $\bar{\sigma}_l p^l$, yield

$$(M^{(1)})^a_\mu t^b \delta_{ab} = -i\sigma_\mu \bar{\sigma}_l k^l \Psi(\rho|q|) \tag{B10}$$

with

$$\Psi(a) \equiv \frac{2\pi^2\rho^4}{\lambda a^2}\left[\frac{4}{a^2} - \frac{4}{3}aK_1(a) - 2K_2(a) + \frac{1}{3}\right]. \tag{B11}$$

Note that if instead a right-handed incoming quark flips its chirality and becomes a left-handed outgoing quark, we only need to conjugate (B11) and substitute $k \longrightarrow -p$. If an instanton is switched to an anti-instanton, then $\sigma \leftrightarrow \bar{\sigma}$ in the final result. With this in mind, we have

$$M^a_\nu t^b \delta_{ab} = -i(\gamma_\mu \not{k} + \not{p}\gamma_\mu)\Psi(\rho|q|) \tag{B12}$$

which is (19).

[1] T. Schafer and E. V. Shuryak, Rev. Mod. Phys. **70**, 323 (1998).
[2] M. Nowak, M. Rho, and I. Zahed, *Chiral Nuclear Dynamics* (World Scientific, Singapore, 1996).
[3] E. Shuryak and I. Zahed, Phys. Rev. D **62**, 085014 (2000).
[4] M. A. Nowak, E. V. Shuryak, and I. Zahed, Phys. Rev. D **64**, 034008 (2001).
[5] E. V. Shuryak and I. Zahed, Phys. Rev. D **69**, 014011 (2004).
[6] D. Kharzeev and E. Levin, Nucl. Phys. **B578**, 351 (2000).
[7] A. E. Dorokhov and I. O. Cherednikov, Nucl. Phys. B, Proc. Suppl. **146**, 140 (2005).
[8] A. Ringwald and F. Schrempp, Phys. Lett. B **503**, 331 (2001); **438**, 217 (1998); "Proceedings, Quarks '94, Vladimir, 1994," p. 170 [arXiv:hep-ph/9411217].
[9] F. Schrempp and A. Utermann, in "Workshop on Strong and Electroweak Matter (SEWM 2002), 2002, Heidelberg, Germany, 2002" [arXiv:hep-ph/0301177]; Acta Phys. Pol. B **33**, 3633 (2002); Phys. Lett. B **543**, 197 (2002).
[10] M. Giordano and E. Meggiolaro, Phys. Rev. D **81**, 074022 (2010); Proc. Sci., LATTICE2011 (2011) 155.
[11] M. Anselmino and S. Forte, Phys. Rev. Lett. **71**, 223 (1993).
[12] N. Kochelev, JETP Lett. **72**, 481 (2000).
[13] A. Dorokhov, N. Kochelev, and W. Nowak, Phys. Part. Nucl. Lett. **6**, 440 (2009).
[14] D. Ostrovsky and E. Shuryak, Phys. Rev. D **71**, 014037 (2005).
[15] A. Airapetian *et al.* (HERMES Collaboration), Phys. Rev. Lett. **84**, 4047 (2000).
[16] A. Airapetian *et al.* (HERMES Collaboration), Phys. Rev. Lett. **94**, 012002 (2005).
[17] A. Airapetian *et al.* (HERMES Collaboration), Phys. Rev. Lett. **103**, 152002 (2009).
[18] H. Avakian *et al.* (CLAS Collaboration), Phys. Rev. Lett. **105**, 262002 (2010).
[19] B. I. Abelev *et al.* (STAR Collaboration), Phys. Rev. Lett. **101**, 222001 (2008).
[20] M. Chiu (PHENIX Collaboration), in *Proceedings of the 17th International Spin Physics Symposium*, AIP Conf. Proc. No. 915 (AIP, New York, 2007), p. 539.
[21] C. Aidala, "Single-Spin Asymmetries and Transverse-Momentum-Dependent Distributions at RHIC" (2011).
[22] D. Adams *et al.* (FNAL E704 Collaboration), Phys. Lett. B **264**, 462 (1991).
[23] D. Sivers, Phys. Rev. D **41**, 83 (1990); **43**, 261 (1991).
[24] J. Collins, Nucl. Phys. **B396**, 161 (1993).
[25] J. Collins, S. Heppelmann, and G. Ladinsky, Nucl. Phys. **B420**, 565 (1994).
[26] S. Moch, A. Ringwald, and F. Schrempp, Nucl. Phys. **B507**, 134 (1997).
[27] A. Airapetian (HERMES Collaboration), Phys. Lett. B **442**, 484 (1998).
[28] Z. Kang, J.-W. Qiu, W. Vogelsang, and F. Yuan, Phys. Rev. D **83**, 094001 (2011).
[29] M. Hirai, S. Kumano, and N. Saito, Phys. Rev. D **74**, 014015 (2006).
[30] M. Glck, E. Reya, and A. Vogt, Eur. Phys. J. C **5**, 461 (1998).
[31] L. Brown, R. D. Carlitz, D. B. Creamer, and C. Lee, Phys. Rev. D **17**, 1583 (1978).
[32] P. Faccioli and E. Shuryak, Phys. Rev. D **64**, 114020 (2001).
[33] S. Vandoren and P. Van Nieuwenhuizen, arXiv:0802.1862.